Tumor Paint: A Chlorotoxin:Cy5.5 Bioconjugate for Intraoperative Visualization of Cancer Foci

Mandana Veiseh,[1] Patrik Gabikian,[2] S-Bahram Bahrami,[1] Omid Veiseh,[3] Miqin Zhang,[2,3] Robert C. Hackman,[1,4] Ali C. Ravanpay,[1,8] Mark R. Stroud,[1] Yumiko Kusuma,[1] Stacey J. Hansen,[1] Deborah Kwok,[1] Nina M. Munoz,[1] Raymond W. Sze,[5] William M. Grady,[6,10,11] Norman M. Greenberg,[1] Richard G. Ellenbogen,[2,9] and James M. Olson[1,4,7,8,9]

[1]Clinical Research Division, Fred Hutchinson Cancer Research Center; Departments of [2]Neurosurgery, [3]Material Science, [4]Pathology, [5]Radiology, [6]Medicine, and [7]Pediatrics, and [8]Program in Neurobiology and Behavior, University of Washington; [9]Children's Hospital and Regional Medical Center; and [10]Puget Sound Health Care System, Seattle, Washington; and [11]Cancer Biology Department, Vanderbilt University Medical School, Nashville, Tennessee

Abstract

Toward the goal of developing an optical imaging contrast agent that will enable surgeons to intraoperatively distinguish cancer foci from adjacent normal tissue, we developed a chlorotoxin:Cy5.5 (CTX:Cy5.5) bioconjugate that emits near-IR fluorescent signal. The probe delineates malignant glioma, medulloblastoma, prostate cancer, intestinal cancer, and sarcoma from adjacent non-neoplastic tissue in mouse models. Metastatic cancer foci as small as a few hundred cells were detected in lymph channels. Specific binding to cancer cells is facilitated by matrix metalloproteinase-2 (MMP-2) as evidenced by reduction of CTX:Cy5.5 binding *in vitro* and *in vivo* by a pharmacologic blocker of MMP-2 and induction of CTX:Cy5.5 binding in MCF-7 cells following transfection with a plasmid encoding MMP-2. Mouse studies revealed that CTX:Cy5.5 has favorable biodistribution and toxicity profiles. These studies show that CTX:Cy5.5 has the potential to fundamentally improve intraoperative detection and resection of malignancies. [Cancer Res 2007;67(14):6882–8]

Introduction

For many types of cancer, the precision of surgical resection directly influences patient prognosis. Unfortunately, intraoperative identification of tumor margins or small foci of cancer cells remains imprecise or depends on surgical judgment. Thus, the extent of surgical resection is constrained by the requirement to avoid harming vital healthy structures. Nowhere is this more problematic than in the brain, where >80% of malignant cancers recur at the surgical margin (1). Despite advances in intraoperative monitoring and image guidance, postoperative scans sometimes reveal bulky residual tumor that may have been resected safely if the surgeon had improved tools to distinguish tumor tissue from normal brain (Supplementary Fig. S1). Recent advances in molecular biology, genomics, and proteomics have yielded information about molecules that are preferentially expressed in malignant cells compared with normal tissue. This information has the potential to fundamentally transform surgical oncology if used to specifically illuminate tumor cells with targeted molecular beacons.

We developed and conducted preclinical evaluation of a molecular imaging bioconjugate composed of chlorotoxin (CTX) and Cy5.5. CTX is a 36 amino acid peptide with four disulfide bridges. CTX is thought to bind to a lipid raft-anchored complex that contains matrix metalloproteinase-2 (MMP-2), membrane type-I MMP, and transmembrane inhibitor of metalloproteinase-2 (TIMP2), as well as ClC-3 chloride ion channels, and other proteins (2, 3). Upon CTX binding, the complex is postulated to be internalized into the cell, eliminating the functional chloride ion channel (2, 3). Several studies showed that CTX binds preferentially to glioma cells compared with non-neoplastic cells or normal brain (2, 4, 5). A radiopharmaceutical bound to synthetic chlorotoxin, ^{131}I-TM-601, showed safety in phase I/II clinical trials for human brain cancer therapy based on an acceptable safety profile in preclinical studies (6).

Cy5.5 is a fluorescent molecular beacon that emits photons in the near-IR (NIR) spectrum. Because photons of this wavelength are minimally absorbed by water or hemoglobin, NIR beacons are well suited for intraoperative imaging (7, 8). Previous attempts to image brain tumors by NIR have focused on targeting the probe to inflammatory microglia around the tumor or using probes that require proteolytic cleavage for activation (9, 10). The former approach is challenging because the presence of microglia correlates poorly, if at all, with margins of many brain tumors. Furthermore, to reduce perioperative brain edema, patients are treated with dexamethasone, which is a potent inhibitor of microglial activation. These factors, coupled with preference for a probe that does not require enzymatic cleavage, prompted us to focus on targeting Cy5.5 directly to cancer cells.

This paper reports the development of CTX:Cy5.5 bioconjugate and the efficacy of this imaging agent in mouse models of glioma, medulloblastoma, prostate cancer, intestinal cancer, and sarcoma. We addressed the sensitivity of CTX:Cy5.5 for detecting cancer foci and metastases noninvasively and under simulated surgical operating conditions and conducted murine biodistribution and toxicity studies. We evaluated the role of MMP-2 in CTX:Cy5.5 binding to cancer cells.

Materials and Methods

Probe synthesis and analysis. Probe was synthesized using a mixture of CTX [Alomone Labs, 2 mg/mL in bicarbonate buffer (pH, 8.5)] and Cy5.5-NHS ester (Invitrogen, 10 mg/mL in anhydrous dimethyl formamide) at the molar ratio of 3:1 (dye/CTX). Conjugation was done in the dark at room temperature for 1 h. Unconjugated dye was removed by dialysis against PBS

Note: Supplementary data for this article are available at Cancer Research Online (http://cancerres.aacrjournals.org/).

M. Veiseh and P. Gabikian contributed equally.

Requests for reprints: James M. Olson, Fred Hutchinson Cancer Research Center, Mailstop D4-100, 1100 Fairview Avenue N., Seattle, WA 98109. Phone: 206-667-7955; Fax: 206-667-2917; E-mail: jolson@fhcrc.org.

doi:10.1158/0008-5472.CAN-06-3948

using Slide-A-Lyzer (Pierce Biotechnology) membrane (M_r cutoff, 3,500) up to 18 h at 4°C. Samples were diluted with PBS to produce 1, 10, and 20 μmol/L of CTX solution and filtered with a 0.2-μm syringe filter before use. All batches were evaluated by mass spectroscopy and Xenogen IVIS-100 to ensure quality.

Cell culture and transfection. 9L rat gliosarcoma cells, MCF-7 human breast adenocarcinoma, and primary human foreskin fibroblast (HFF; American Type Culture Collection) were maintained in DMEM, MEM, and RPMI supplemented with 1% sodium pyruvate, 1% streptomycin/penicillin and 10% fetal bovine serum (Hyclone), respectively. For transfection experiments, MCF-7 cells were trypsinized, replated at a 10,000- to 12,000-cell/mL density, and cultured 12 to 16 h before transfection. MCF-7 cells were transfected with MMP-2 or an empty vector along with pMacs4.1 (Miltenyi Biotec) using FuGENE 6 Transfecton Reagent (Roche) according to manufacturer's instructions.

***In vitro* imaging.** A total of 20,000 cells were seeded on sterile coverslips 36 h before labeling and confocal microscopy. Cells were cultured with 1 mL of CTX:CY5.5 conjugate (1 μmol/L) for 2 h in a 37°C humidified incubator maintained at 5% CO_2. Following this step, cell membranes were stained with 1 μmol/L solution of FM 1-43FX (Invitrogen) for 20 min in the dark at room temperature, washed twice in PBS, and fixed in 4% paraformaldehyde. A final treatment with prolong gold antifade solution (Invitrogen) containing 6-diamidino-2-phenylindole (DAPI)–stained cellular nuclei and preserved the fluorescence of the samples for confocal microscopy. Confocal images were acquired using a DeltaVision SA3.1 wide-field deconvolution microscope (Applied Precision) equipped with DAPI, TRITC, and Cy5 filters. Confocal image processing was done using SoftWoRX (Applied Precision).

Animal models. All mouse studies were conducted in accordance with the Institute of Animal Care and Use Committee–approved protocols. S.c. xenografts were established in *nu/nu* (Charles River) mice using 9L, a rat gliosarcoma cell line, and RH30, a rhabdomyosarcoma cell line. The xenografts were established using 1 million 9L or RH30 cells suspended in serum-free media and Matrigel (BD Biosciences) at a 1:1 ratio. Intracranial xenografts were established by stereotaxic injection of 1 million 9L cells suspended in 10 μL PBS into the brain 3 mm lateral and posterior to the bregma. ND2:SmoA1 medulloblastoma mice, TRAMP prostate cancer mice and Apc^{1638N} intestinal adenoma and adenocarcinoma mice were previously described (11–14).

Blood-brain barrier analysis. The blood-brain barrier integrity in SmoA1 and control mice was assessed by injection of 100 μL of Evan's Blue dye into tail veins 2 h before sacrifice and perfusion with PBS. Whole organs were removed from perfused animals and photographed without further processing (15).

The integrity of the blood-brain barrier was also evaluated using albumin immunostaining as previously described (16). Briefly, 10-μm sections were generated from paraffin-embedded blocks of unperfused brains of 2-month-old symptomatic SmoA1 mice. These sections contain tumor within the cerebellum surrounded by normal cerebellar and cortical tissue. The sections were deparaffinized and rehydrated. Endogenous peroxidase was blocked using 0.3% hydrogen peroxidase in methanol for 10 min. The sections were incubated in 1% gelatin (cold water skin fish, Sigma Co.) for 30 min followed by goat anti-mouse albumin antibody (1:10,000 dilution, Bethyl Laboratories Inc.) for 1 h at ambient temperature. The sections were washed in PBS and incubated with biotinylated anti-goat immunoglobulin G (IgG) antibody (Bio-Rad at 1:250) for 30 min. The staining was visualized using the DAB system (Pierce).

***In vivo* imaging.** CTX:Cy5.5 (0.1–0.2 mL of 10–20 μmol/L) was given i.v. by tail vein injection. Biophotonic images were obtained on the Xenogen IVIS-100 system (Xenogen). Mice were anesthetized with 1% to 2.5% isoflurane (VEDCO, Inc.) before they were placed in the imaging chamber and imaged at various time points postinjection. Relevant organs and tumors were dissected from some of the animals and imaged immediately following dissection. In time course experiments, all images were captured using identical system settings, and fluorescence emission was normalized to photons per second per centimeter squared per steradian ($p/s/cm^2/sr$). All experiments were repeated multiple times, and representative images are shown in the figures. For unconjugated Cy5.5 control experiments, the NHS ester–reactive group, which is absent in CTX:Cy5.5 was reduced by solubilizing Cy5.5-NHS ester in water adjusted to pH 9 for 90 min then buffered in PBS. Before injection, the NIR fluorescent emission of equimolar concentrations of CTX:Cy5.5 and Cy5.5 were compared on filter paper to ensure that fluorescence was not quenched. For CTX blocking experiments, 7-day Alzet pumps were loaded with 2 mmol/L unconjugated CTX and implanted s.c. near the scapula. The next day, 30 μL of 20 μmol/L CTX:Cy5.5 plus 70 μL of 2 mmol/L unconjugated CTX was injected into tail veins. Control animals received vehicle instead of CTX. Imaging was done daily from days 1 to 4.

Statistical analyses. Statistical analyses used the paired t test after it was determined in the largest data set ($n = 22$) that the values had a normal distribution. Paired t test was used in instances where tumor tissue was compared with normal tissue in the same animal rather than between animals, and unpaired t test was used to analyze comparisons between groups of animals.

Gelatin zymography. Gelatin zymography was done using previously published protocol (17). Briefly, 24 h before initiation of assay, cell growth media were switched to serum-free media. At time of sample preparation, media was aspirated, and proteins were concentrated using Microcon (Millipore) centrifuge filters of 10,000 nominal molecular weight limits. Cells were lysed in SDS-sample buffer containing 1% Triton X-100. Concentrated media and cell lysate samples were loaded at a concentration of 15 μg/μL without reduction on 10% SDS-PAGE gel containing 1% gelatin. The gels were washed with 2.5% Triton X-100 after electrophoresis and were incubated overnight in the developing buffer at 37°C to induce gelatin lysis. The resultant gelatinase activity was qualitatively determined by Coommassie counterstaining.

Western assay. Western analyses were conducted per standard procedure using 2 μg/mL antihuman MMP-2 antibody (Chemicon) that has cross-reactivity against rat MMP-2 antigen and developed using Lumi-Light chemiluminescence system (Roche).

Pulldown assay. Recombinant MMP-2 (Chemicon; 1 μL of 0.1 mg/mL) was incubated with Ctx-Cy5.5 or Cy5.5 (25 μL of 20 μmol/L) in 500 μL phosphate buffer saline (PBS Life Technologies) at 37°C for 2 h. Bovine serum albumin (Sigma) was used as a control for nonspecific binding to MMP-2. Primary antihuman MMP-2 antibody (Chemicon, 2 μg/mL) was added and incubated at 4°C overnight. Fresh protein G sepharose (Amersham Bioscience; 5 μL of 10%) was added, and samples were incubated for 2 h at 4°C. The samples were centrifuged at 8,000 rpm for 5 min at 4°C, and supernatants were collected. Protein G immunoprecipitate was washed thrice in 0.5 mL PBS and resuspended in PBS (1:1). Samples were spotted (5 μL) and imaged on Xenogen IVIS-100 system.

Mass spectroscopy. CTX:Cy5.5 (1 μmol/L) was incubated with media of the 9L and U87 cells at 37°C for 2 h to resemble the *in vitro* cell culture condition. The samples were analyzed on a Voyager DE-Pro MALDI-TOF mass spectrometer (Applied Biosystems) in the positive ion mode. A calibration mixture of PepMix3 [apomyoglobin (horse) and bovine insulin] was first analyzed to calibrate the instrument, and the samples were mixed with sinapinic acid before analysis.

Immunostaining. CTX:Cy5.5-treated cells were fixed (4% paraformaldehyde in PBS for 30 min), permeabilized [Triton X-100 treatment (0.1% in PBS) for 10 min], and blocked [5% (w/v) solution of nonfat dry milk in PBS with 0.1% Tween 20 for 30 min] before incubation with antihuman MMP-2 antibody (amino acids 468–483 hMMP-2, clone 42-5D11; Chemicon; 2 μg/mL overnight at 4°C). The samples were washed thrice with blocking buffer before the secondary antibody treatment (goat anti-mouse IgG (H + L); Jackson ImmunoResearch; manufacturer's recommended concentration for 1 h at room temperature in the dark). The samples were washed with PBS thrice and blown dry with air and mounted with Prolong Gold antifade solution containing DAPI for cellular nuclei staining and fluorescence preservation.

Histology and microscopy. For mouse experiments, tissues were fixed in freshly prepared 4% paraformaldehyde and stained with H&E per standard clinical laboratory protocol. Confocal microscopy was done on freshly harvested tissues using a Zeiss LSM 510 (Carl Zeiss) microscope via 633-nm HeNe laser lines for excitation and 650 to 710 nm bandpass filter for emission collection through a photomultiplier tube capturing system. NIR signal was translated into red pseudocolor to enable detection in the visible spectrum.

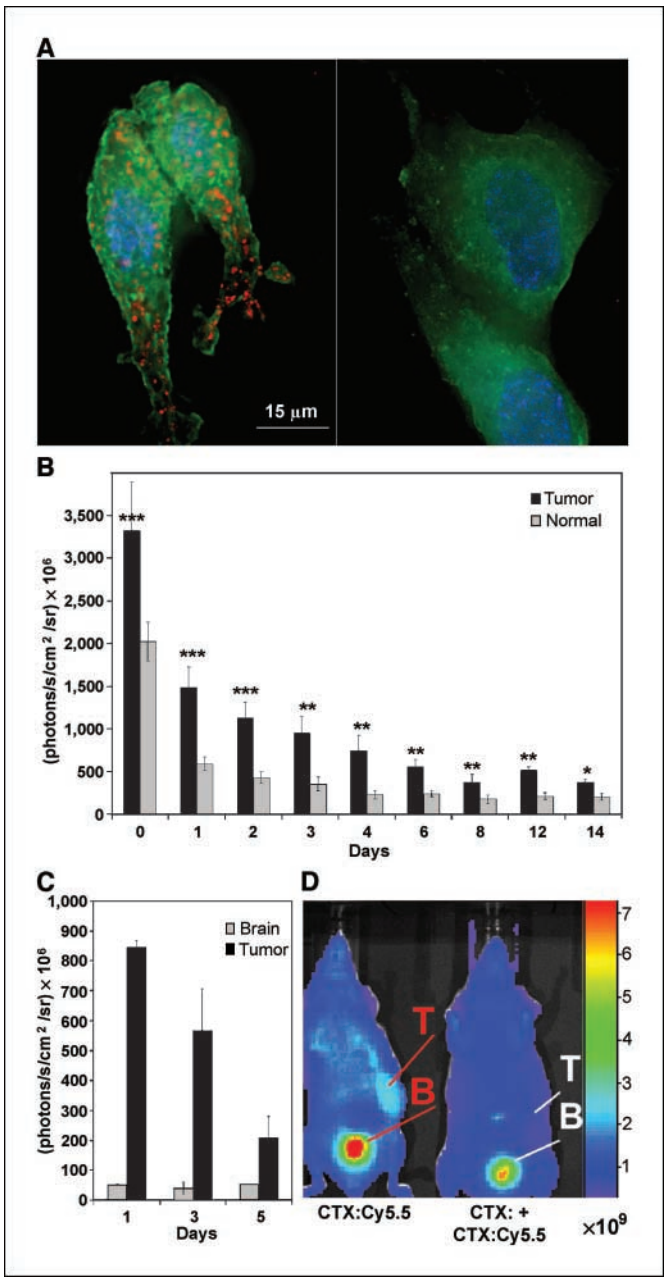

Figure 1. Biophotonic imaging of glioma. *A,* CTX:Cy5.5 bioconjugate emits signal from every 9L glioma cell in culture (*left*), but minimal signal from fibroblasts, indicating tumor cell-specific binding (*right*). *B,* following administration of CTX:Cy5.5, NIRF signal is significantly higher in 9L glioma xenografts than in normal tissue at all time points through day 14. ***, $P < 0.0005$; **, $P < 0.005$; and *, $P < 0.05$. *Columns,* mean; *bars,* SE. *C, ex vivo* imaging of 9L glioma xenograft tumors showed higher signal than normal brain ($P < 0.001$) at all time points by *t* test, $n = 3$. *Columns,* mean; *bars,* SE. *D,* CTX:Cy5.5 binding in tumor (*T*) is blocked by coadministration of unlabeled chlorotoxin (*right*) compared with mouse that received CTX:Cy5.5 with no unlabeled chlorotoxin (*left*). These photographs are from the ventral surface of the mouse, so CTX:Cy5.5 that is eliminated by renal excretion is seen in the bladder (*B*).

Results

Biophotonic imaging of glioma. CTX:Cy5.5 bioconjugate was incubated with 9L glioma cells and primary fibroblasts, and binding was evaluated by near infrared fluorescence (NIRF) microscopy. All 9L glioma cells exposed to CTX:Cy5.5 emitted signal in the NIRF spectrum (Fig. 1*A, left*), whereas minimal signal was detected from fibroblasts treated with the same concentration of probe (Fig. 1*A, right*). We assessed the *in vivo* activity of CTX:Cy5.5 noninvasively in 22 mice with 9L glioma xenografts. Following tail vein injection of 0.1 mL of 20 μmol/L bioconjugate, the probe distributed rapidly throughout the body. At all time points through 14 days after injection, NIRF emission was higher in xenografts than in non-neoplastic tissue ($P < 0.0005$ on days 0–2; 0.005 on days 3–12; and <0.05 on day 14; Fig. 1*B*). Because autofluorescence is lower in the brain than flank, we studied the ratio of CTX:Cy5.5 signal in the brain compared with glioma xenografts. As anticipated, mice bearing 9L glioma flank xenografts sacrificed 1, 3, and 5 days after bioconjugate injection revealed significantly increased signal in tumor compared with brain at all time points ($P < 0.001$, Fig. 1*C*).

To determine whether the tumor-specific signal was due to CTX:Cy5.5 binding to the CTX binding site versus the enhanced permeability and retention (EPR) effect, we tested whether unlabeled chlorotoxin could block CTX:Cy5.5 signal in tumor. In these experiments, signal was blocked in tumor by the coadministration of chlorotoxin (Fig. 1*D*). To further assess the targeting role of CTX, the tumor-specific signal in mice injected with Cy5.5 was compared with those of CTX:Cy5.5 at days 0 and 1 postinjection (Supplementary Fig. S2*A* and *B*). The tumor-specific signal in CTX:Cy5.5-injected mice was significantly higher than uninjected controls and Cy5.5-injected mice. The difference between Cy5.5-injected mice and uninjected controls was not significant at either time point (Supplementary Fig. S2*C*).

As predicted by the s.c. xenograft model, brain xenograft experiments confirmed a clear distinction between tumor and normal brain (Supplementary Fig. S2*D*).

The specificity of CTX:Cy5.5 for tumor compared with non-neoplastic tissue seems to be directly attributable to the targeting role of CTX because signal intensity from CTX:Cy5.5-treated 9L glioma cells was remarkably higher than Cy5.5-treated cells under identical treatment conditions (1 μmol/L, 2 h at 37°C; Supplementary Fig. S2*E* and *F*).

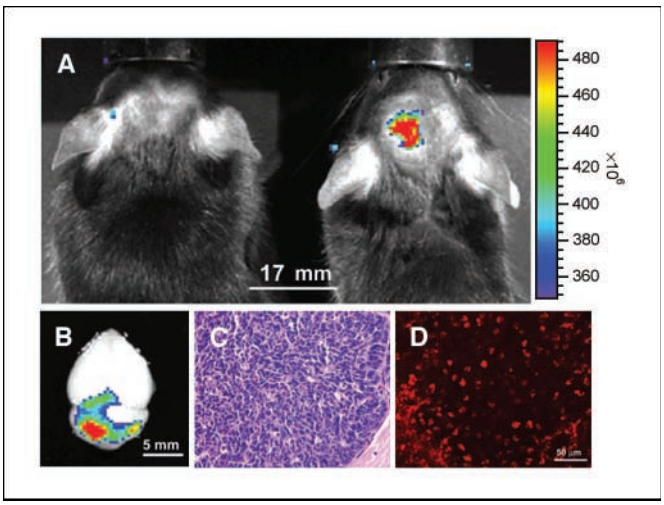

Figure 2. Detection of autochthonous medulloblastoma in genetically engineered mice. *A,* biophotonic images of tumor-free wild-type mouse (*left*) and ND2:SmoA1 mouse (*right*). Mice were injected with 0.2 mL of 10 μmol/L probe 1.5 d before imaging. Representative sample shown from five mice with similar results. *B,* images of brains from the same mice following necropsy confirms signal from tumor. *C,* histologic confirmation of medulloblastoma tumor. *D,* confocal microscopy images from the same brains shown in (*B*) demonstrating the near absence of Cy5.5 signal in control and presence in medulloblastoma.

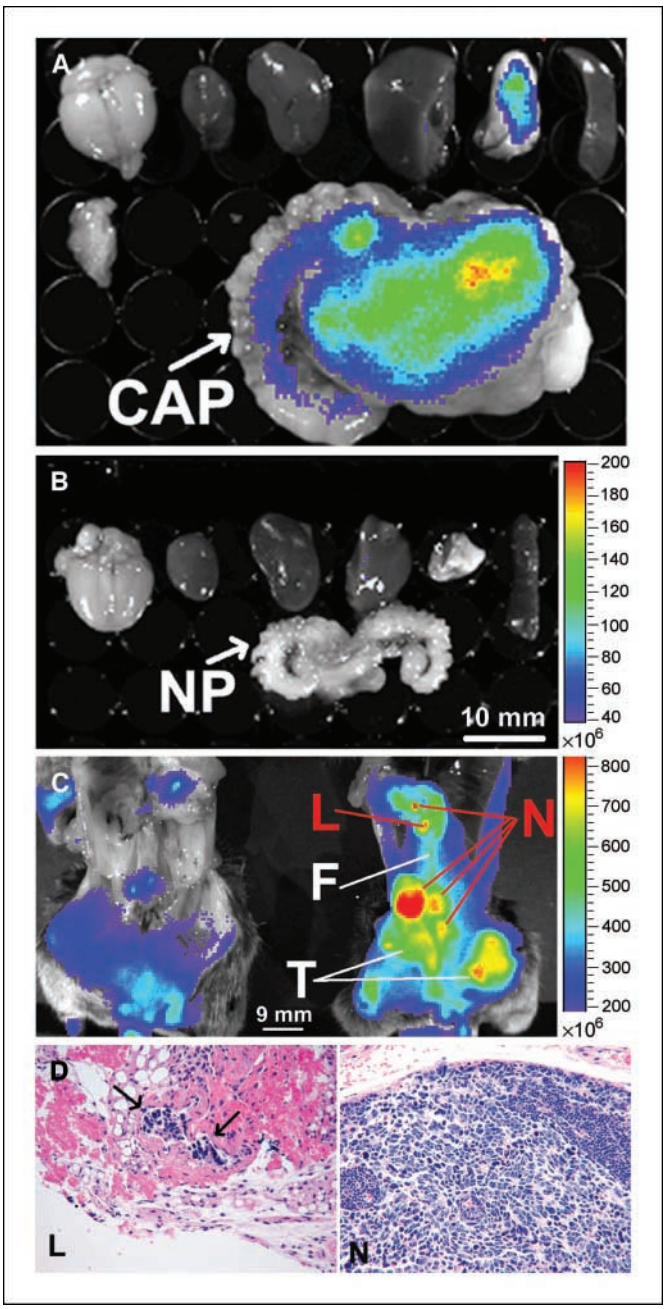

Figure 3. Specificity of CTX:Cy5.5 for human and mouse prostate cancer. *A,* biophotonic image of prostate and other organs from TRAMP mouse. *CAP*, cancerous prostate. *B,* wild-type control shows specific signal in TRAMP prostate and lung. Representative image from three animals in each group. Images were obtained 5 d after injection of 0.1 mL of 10 μmol/L probe. *Top row,* brain, heart, kidney, liver, lung, and spleen. *Bottom row, NP*, normal prostate. *C,* intraoperative images of control (*left*) and TRAMP (*right*) mouse abdomen following removal of intestine, prostate, and liver. Multiple lymph nodes (*N*) were positive by biophotonic imaging and histology. A 1.5-mm-diameter tissue nodule that was very bright on imaging revealed a small focus of prostate cancer cells in lymph channels surrounded by fat and reactive tissue (*L*). Lower amounts of signal were detected in fat (*F*) and testes (*T*). *D,* H&E stain showing cancer focus in lymph channel and cancer packed lymph node (data not shown).

Noninvasive imaging of medulloblastoma through cranial bone. We tested CTX:Cy5.5 in the SmoA1 genetically engineered autochthonous mouse model of medulloblastoma (11). In these mice, medulloblastomas arise in the cerebellum due to transgenic expression of constitutively active smoothened, a mediator of sonic hedgehog activity. Tumors were detected through intact skull and scalp, and the level of NIRF emission grossly reflected tumor size (Fig. 2*A* and *B* and data not shown). Histologic analysis confirmed tumor presence in mice that exhibited the signal following CTX:Cy5.5 (Fig. 2*C*), and confocal microscopy of *ex vivo* tumor specimens revealed bright staining of medulloblastoma cells with CTX:Cy5.5 (Fig. 2*D*). Two approaches were used to establish that the blood-brain barrier was intact in SmoA1 mice. Albumin immunostaining showed that the albumin was limited to intravascular space in normal brain and medulloblastoma of SmoA1 mice (Supplementary Fig. S3*A*), and Evans blue dye was excluded from brain and tumor parenchyma in SmoA1 mice (Supplementary Fig. S3*B* and *C*). Because these tumors arise in the absence of blood-brain barrier disruption, we conclude that CTX:Cy5.5 enters the mouse medulloblastoma tissue at concentrations suitable for real-time imaging, and that intracranial tumors can be readily detected noninvasively.

Imaging of mouse prostate cancer, intestinal cancer, and sarcoma. At the time imaging studies were conducted, we were operating under the assumption that MMP-2 was the CTX target. To determine whether CTX:Cy5.5 illuminated cancer foci of MMP-2–positive tumors that were not of neuroectodermal origin, we conducted studies in transgenic mice that express the SV40T gene in prostate epithelium (12, 18). In these mice, CTX:Cy5.5 illuminated the primary prostate cancer as well as lung metastases (Fig. 3*A* and *B*). CTX:Cy5.5 binding correlated with the histologic presence of neoplastic cells in the primary (Supplementary Fig. S4*A–D*) and distant organs (data not shown). Under simulated surgical conditions, microscopic foci of cancer cells in lymphatic channels and lymph nodes were easily detected (Fig. 3*C–D*).

We next assessed NIR emission in a genetically engineered familial adenomatous polyposis (FAP) model, the Apc^{1638N} mouse, and in a xenograft sarcoma model. In Apc^{1638N} mice, intestinal neoplasms could not be resolved by noninvasive NIRF imaging because of autofluorescence of alfalfa-containing intestinal contents. However, *ex vivo* analysis of the intestine that was free of intestinal contents showed exquisite delineation of 3- to 5-mm diameter cancer nodules and no appreciable signal from otherwise normal intestine (Fig. 4*A–C*). Biophotonic (Fig. 4*D*) and confocal analyses (Supplementary Fig. S5*A–C*) of Rh30 rhabdomyosarcoma xenografts showed that CTX:Cy5.5 targets this type of tumor as well.

Biodistribution and toxicity. CTX has previously been administered to human patients in clinical trials, but the pharmacokinetic properties of the bioconjugate have not been previously reported (6, 19). Unbound bioconjugates were fairly evenly distributed through the mouse body during the first 24–96 h, with the exception that NIR emission from kidney was much higher than any other organ (Fig. 5). Confocal microscopy showed that CTX:Cy5.5 was concentrated in the renal collecting system as expected for a compound that is primarily excreted in urine (data not shown).

In many cases, scorpion venom peptides are selectively toxic to particular insects or higher organisms and nontoxic to others. CTX causes paralysis in crayfish, but no toxicity has been reported in mammals. In our study, mice that were injected with CTX:Cy5.5 were indistinguishable from control mice in open-field observation (data not shown). To further assess potential CTX:Cy5.5 toxicity at doses used for optical imaging, complete necropsy was done on mice 2 weeks after exposure to CTX:Cy5.5. Brain, heart, lungs,

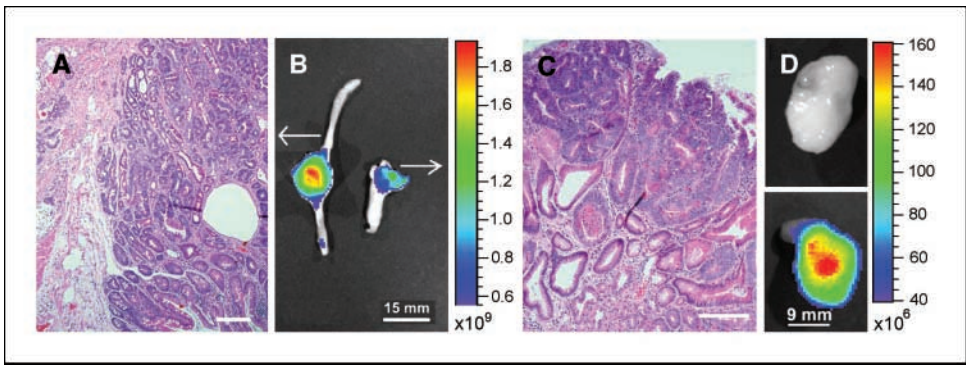

Figure 4. CTX:Cy5.5 imaging of adenocarcinomas and sarcomas. *A–C,* biophotonic image of adenocarcinoma (*B, left*) and adenoma (*B, right*) shows clear delineation from normal intestine. Histologic confirmation of (*A*) adenocarcinoma and (*C*) adenoma. *D, ex vivo* image of Rh30 xenograft from uninjected (*top*) and CTX:Cy5.5-injected (*bottom*) animals shows probe-specific signal.

kidneys, liver, spleen, and skin were indistinguishable from control mice on gross inspection and histology (data not shown). Laboratory evaluation showed no alteration in hematocrit, platelet count, WBC count, electrolytes, liver function, or kidney function (data not shown). We conclude that, at doses used for optical imaging, no toxicity from CTX:Cy5.5 could be detected in mice.

MMP-2 facilitates CTX:Cy5.5 binding. The MMP-2 molecular complex is the leading candidate target for CTX (2, 3). To determine whether MMP-2 is also involved in CTX:Cy5.5 tumor cell targeting, we evaluated CTX:Cy5.5 binding in the presence and absence of an MMP2 inhibitor. Binding of CTX:Cy5.5 to 9L glioma cells in culture was blocked by preincubation with (50 μmol/L) of the MMP inhibitor, 1,10-phenanthroline (Sigma Aldrich; data not shown). Specific binding of CTX:Cy5.5 was 6-fold lower when mice with 9L glioma xenografts were pretreated with 1,10-phenanthroline, indicating that imaging reflected binding of CTX:Cy5.5 to tumor cells rather than simply measuring increased blood flow in neovascularized tumors (Fig. 6*A*). Although these studies indicated that MMPs were involved in CTX:Cy5.5 binding, further experiments were necessary to elucidate the role of MMP-2 because MMP inhibitors may have off-target activity.

To determine by genetic means whether MMP-2 is involved in CTX:Cy5.5 binding, we transfected MCF7 cells, which express low levels of MMP-2 and bind CTX:Cy5.5 poorly in comparison to other cell lines (20) with a plasmid encoding MMP-2. Transfected cells were sorted from untransfected cells. Increased MMP-2 levels in transfected cells were confirmed by indirect immunofluorescence (Fig. 6*B, right,* and *D*) and confirmed by Western blot and gelatinase assays (data not shown). MMP-2–transfected cells (Fig. 6*B, right*). showed higher CTX:Cy5.5 binding than control plasmid-transfected cells (Fig. 6*B, left*). Confocal microscopy showed CTX:Cy5.5 and MMP-2 colocalization in transfected cells (Fig. 6*C* and *D*). We reasoned that if MMP-2 was important for CTX:Cy5.5 binding, then all of the tumors that bind CTX:Cy5.5 should show MMP-2 activity. Indeed, Western blot analyses, gelatinase assays, and indirect immunofluorescence assays revealed that the mouse tumors and cell lines used in the experiments reported above were MMP-2 positive (Supplementary Table S1).

These experiments showed that CTX:Cy5.5 binding was facilitated by MMP-2, but did not establish whether it specifically binds the bioconjugate. To assess this, we evaluated binding between CTX:Cy5.5 and recombinant MMP-2 using pulldown experiments. In six pulldown experiments, there was no clear evidence that CTX:Cy5.5 binds to MMP-2 in a specific manner. In the example shown, the amount of bioconjugate pulled down by a monoclonal antibody against MMP-2 and protein G was similar whether recombinant MMP-2 or bovine serum albumin was included (Supplementary Fig. S6). CTX:Cy5.5 incubated at 37°C in the media of 9L or U87 cells showed no change in mass compared with CTX:Cy5.5, indicating that the bioconjugate is not enzymatically altered by MMP-2 (data not shown). Taken together with the pharmacologic inhibition and transfection studies, these data indicate that MMP-2 is important for CTX:Cy5.5 binding to cancer cells, but the two molecules may not specifically bind to each other. The exact molecular target of CTX:Cy5.5 needs further investigation in the context of MMP-2 macromolecular complex.

Discussion

Surgery remains a principal component of cancer therapy. Despite advances in surgical guidance tools, delineation of the tumor/normal tissue interface continues to rely on color, texture, or vascularity differences that are often subtle and imperfect. Insufficient visual cues between tumor and normal tissue contribute to potentially preventable cancer progression or unacceptable morbidity when too little or too much tissue is resected. The technique described here combines an intuitive visual guide for the surgeon with the potential for significant improvement in accuracy and safety by virtue of its molecular precision.

CTX:Cy5.5 bioconjugate enables real-time biophotonic imaging of malignant cancer foci as small as a few hundred cells. In our studies of more than 50 mice, all tissues sent to pathology tagged as cancer based on CTX:Cy5.5 signal were cancerous, and all adjacent normal tissues were histologically normal. The resolution of cancer foci from normal tissue under simulated operating conditions was exquisite.

CTX:Cy5.5 enabled detection and monitoring of a variety of cancers in mouse models. This approach adds particular value to genetically engineered mouse (GEM) models that develop *in situ* cancers as a result of genetic manipulation that recapitulates human disease. A particular advantage of GEM models is that tumors can be studied from early to advanced stages to better understand the evolution of growth, angiogenesis, local invasion, metastases, drug response, and drug resistance. The ability to detect early-stage tumors for molecular or therapeutic studies can be dramatically improved by a real-time imaging technique such as the one reported here (21, 22).

In this and a related study, we show that CTX:Cy5.5 is superior to CTX conjugates with other NIR tags and to Cy5.5 alone.[12] Our roup previously reported technology for linking CTX to nanoparticles, although further optimization is required to achieve tumor-specific

[12] M. Veiseh, unpublished data.

binding *in vivo* (23). Tumor specificity is also much higher for CTX:Cy5.5 than previously reported for radiolabeled unconjugated CTX (6). In our opinion, the most likely reason is that the pharmacokinetic properties of CTX:Cy5.5 are favorable compared with the other molecules. An unexpected and welcome finding of the current study was the long duration of probe activity, which permits imaging long after peak serum levels have subsided. The observation that gliomas were distinguishable from normal tissue for 14 days after bioconjugate injection bodes well for the utility of this agent in human patients.

Radiolabeled CTX has been safely administered to patients as a potential therapeutic agent for treating gliomas (6). This is consistent with the absence of neurotoxicity in previous mouse studies, including one that involved direct injection of CTX into mouse brain (5, 19). In the current study, CTX:Cy5.5 crossed the blood-brain barrier to bind to autochthonous medulloblastoma foci, but showed minimal signal above background in normal brain structures. Treated animals exhibited no neurologic or behavioral deficits, and postmortem studies revealed no evidence of neuropathology. We observed no pathologic changes in other organs and no alteration of electrolytes, blood counts, or kidney and liver function tests. These data support further toxicity testing in other species in preparation for future human clinical trials.

MMP-2 (gelatinase) is a proteolytic enzyme that degrades extracellular matrix (ECM) during embryologic development and cancer invasion of normal tissue (24, 25). MMP-2 is activated by MTI-MMP, inhibited by TIMP-2, and is thought to act upon $\alpha v\beta 2$ integrin, which facilitates cell adherence to the ECM. All four of these molecules localize to lipid rafts or caveolae that provide a structure for regulated activity on the ECM (26). The importance of this interaction between MMP-2 and caveolae components is supported by changes in MMP-2 expression and metastatic potential following mutations in caveolin components (27).

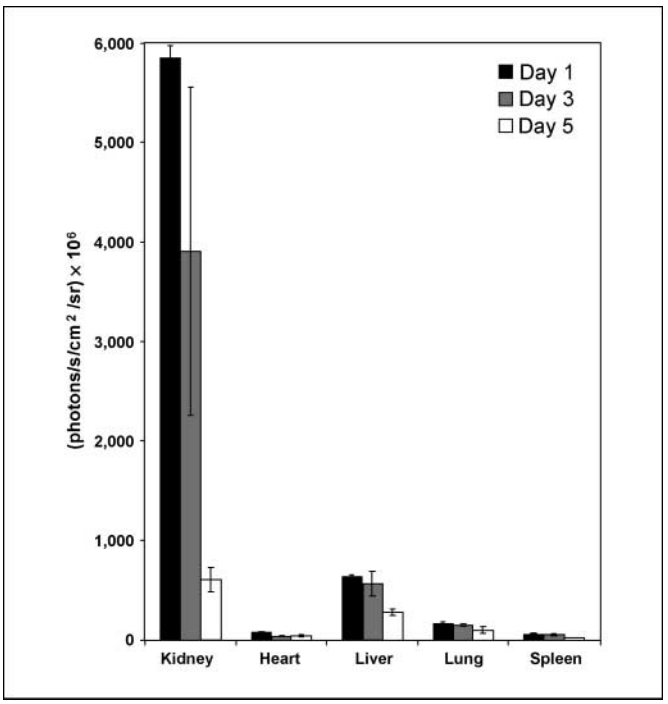

Figure 5. Biodistribution analysis. Signal in normal organs at 1, 3, and 5 d after injection of 100 μL of 20 μmol/L CTX:Cy5.5. *Columns,* mean of three replicates; *bars,* SE.

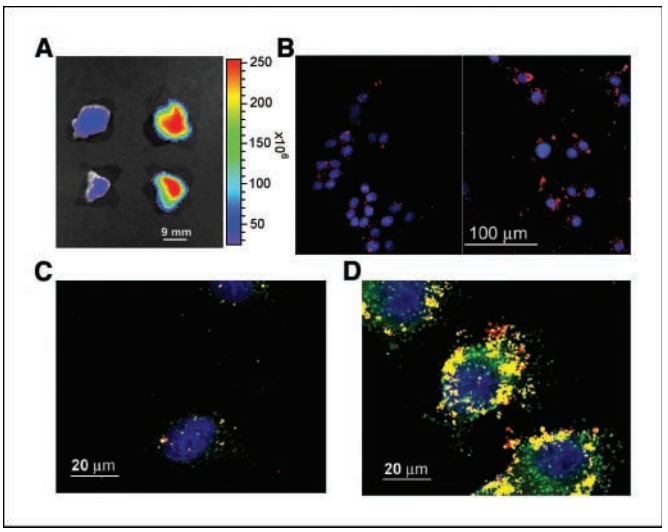

Figure 6. MMP-2 and CTX:Cy5.5 trafficking. *A,* inhibition of CTX:Cy5.5 binding by the MMP-2 blocker in 9L glioma xenograft tumor, 1,10-phenanthroline (*left, top* and *bottom*) compared with binding in control mice that did not receive 1,10-phenanthroline (*right*). *B,* mock-transfected MCF7 cells (*left*) and MCF7 cells transfected with a plasmid encoding MMP-2 (*right*) by NIRF microscopy after 2 h incubation with 1 μmol/L CTX:Cy5.5 (*red*) and DAPI nuclear stain (*blue*). Shown are representative images from three independent experiments. *C* and *D,* confocal images of (*C*) mock-transfected and (*D*) MMP-2–transfected MCF7 cells showing staining with MMP-2 antibody (*green*), CTX:Cy5.5 (*red*), and colocalization of both (*yellow*) and DAPI (*blue*).

Consistent with previous studies, our data indicate that CTX:Cy5.5 binding to cancer cells is MMP-2 dependent, based on reduced CTX:Cy5.5 binding in the presence of MMP2 inhibitors and increased CTX:Cy5.5 binding in cells that were transfected with a plasmid encoding MMP2. These studies are consistent with a model in which CTX targets a component of the MMP2 complex that is anchored in lipid rafts (3). The specific role of MMP2 in targeting and trafficking remains to be elucidated.

Radiolabeled CTX has been safely administered to patients and has been reported to target gliomas approximately 1.3-fold higher than in adjacent brain tissue (5, 6). In our studies, tumor-specific binding was substantially higher than observed with unconjugated CTX, and no toxicity was evident. It is possible that the Cy5.5 moiety improves tumor-specific targeting. The clear delineation between tumor and normal tissue is ideal for real-time surgical biophotonic imaging, particularly for identification of residual tumor following standard surgical resection. For cancers in which the extent of surgical resection correlates with survival, the advancement of CTX:Cy5.5 to human clinical trial offers an opportunity to improve cancer survivorship with minimal or no added toxicity.

Acknowledgments

Received 10/26/2006; revised 3/27/2007; accepted 5/16/2007.

Grant support: NIH grants N01 C037007-16 (R.W. Sze, M. Zhang, J.M. Olson) and CA84296 (N.M. Greenberg); the Seattle Children's Hospital and Regional Medical Center Brain Tumor Research Endowment (R.G. Ellenbogen, J.M. Olson, M. Zhang); and the Fred Hutchinson Cancer Research Center Core Grant (W.M. Grady). Scientific Imaging shared resource is funded by NIH core grant P30 CA15704-31.

The costs of publication of this article were defrayed in part by the payment of page charges. This article must therefore be hereby marked *advertisement* in accordance with 18 U.S.C. Section 1734 solely to indicate this fact.

We thank Sally Ditzler, Barbara Pullar, Jennifer Stoeck, Claire Gibson, Linda Cherepow, Daniel Silbergeld, Julio Vazquez, Dave McDonald, and Adrian Quintanilla for experimental assistance and Andrew Hallahan, Stephan Tapscott, and J. Russel Geyer for helpful discussion.

References

1. Barker FG II, Chang SM, Gutin PH, et al. Survival and functional status after resection of recurrent glioblastoma multiforme. Neurosurgery 1998;42:709–20.
2. Deshane J, Garner CC, Sontheimer H. Chlorotoxin inhibits glioma cell invasion via matrix metalloproteinase-2. J Biol Chem 2003;278:4135–44.
3. McFerrin MB, Sontheimer H. A role for ion channels in glioma cell invasion. Neuron Glia Biol 2006;2:39–49.
4. Lyons SA, O'Neal J, Sontheimer H. Chlorotoxin, a scorpion-derived peptide, specifically binds to gliomas and tumors of neuroectodermal origin. Glia 2002;39:162–73.
5. Soroceanu L, Gillespie Y, Khazaeli MB, Sontheimer H. Use of chlorotoxin for targeting of primary brain tumors. Cancer Res 1998;58:4871–9.
6. Hockaday DC, Shen S, Fiveash J, et al. Imaging glioma extent with ^{131}I-TM-601. J Nucl Med 2005;46:580–6.
7. Bremer C, Ntziachristos V, Weissleder R. Optical-based molecular imaging: contrast agents and potential medical applications. Eur Radiol 2003;13:231–43.
8. Mahmood U, Weissleder R. Near-infrared optical imaging of proteases in cancer. Mol Cancer Ther 2003;2:489–96.
9. Kircher MF, Mahmood U, King RS, Weissleder R, Josephson L. A multimodal nanoparticle for preoperative magnetic resonance imaging and intraoperative optical brain tumor delineation. Cancer Res 2003;63:8122–5.
10. Ntziachristos V, Tung CH, Bremer C, Weissleder R. Fluorescence molecular tomography resolves protease activity *in vivo*. Nat Med 2002;8:757–60.
11. Hallahan AR, Pritchard JI, Hansen S, et al. The SmoA1 mouse model reveals that notch signaling is critical for the growth and survival of sonic hedgehog-induced medulloblastomas. Cancer Res 2004;64:7794–800.
12. Greenberg NM, DeMayo F, Finegold MJ, et al. Prostate cancer in a transgenic mouse. Proc Natl Acad Sci U S A 1995;92:3439–43.
13. Fodde R, Edelmann W, Yang K, et al. A targeted chain-termination mutation in the mouse Apc gene results in multiple intestinal tumors. Proc Natl Acad Sci U S A 1994;91:8969–73.
14. Kaplan-Lefko PJ, Chen TM, Ittmann MM, et al. Pathobiology of autochthonous prostate cancer in a preclinical transgenic mouse model. Prostate 2003;55:219–37.
15. Belayev L, Saul I, Busto R, et al. Albumin treatment reduces neurological deficit and protects blood-brain barrier integrity after acute intracortical hematoma in the rat. Stroke 2005;36:326–31.
16. Zea-Aragon Z, Terada N, Ohno N, et al. Effects of anoxia on serum immunoglobulin and albumin leakage through blood-brain barrier in mouse cerebellum as revealed by cryotechniques. J Neurosci Methods 2004;138:89–95.
17. Deryugina EI, Bourdon MA, Luo GX, Reisfeld RA, Strongin A. Matrix metalloproteinase-2 activation modulates glioma cell migration. J Cell Sci 1997;110:2473–82.
18. Huss WJ, Maddison LA, Greenberg NM. Autochthonous mouse models for prostate cancer: past, present and future. Semin Cancer Biol 2001;11:245–60.
19. Shen S, Khazaeli MB, Gillespie GY, Alvarez VL. Radiation dosimetry of ^{131}I-chlorotoxin for targeted radiotherapy in glioma-bearing mice. J Neurooncol 2005;71:113–9.
20. Giambernardi TA, Grant GM, Taylor GP, et al. Overview of matrix metalloproteinase expression in cultured human cells. Matrix Biol 1998;16:483–96.
21. Graves EE, Weissleder R, Ntziachristos V. Fluorescence molecular imaging of small animal tumor models. Curr Mol Med 2004;4:419–30.
22. Hielscher AH. Optical tomographic imaging of small animals. Curr Opin Biotechnol 2005;16:79–88.
23. Veiseh O, Sun C, Gunn J, et al. Optical and MRI multifunctional nanoprobe for targeting gliomas. Nano Lett 2005;5:1003–8.
24. Cox G, O'Byrne KJ. Matrix metalloproteinases and cancer. Anticancer Res 2001;21:4207–19.
25. Rao JS. Molecular mechanisms of glioma invasiveness: the role of proteases. Nat Rev Cancer 2003;3:489–501.
26. Puyraimond A, Fridman R, Lemesle M, Arbeille B, Menashi S. MMP-2 colocalizes with caveolae on the surface of endothelial cells. Exp Cell Res 2001;262:28–36.
27. Williams TM, Medina F, Badano I, et al. Caveolin-1 gene disruption promotes mammary tumorigenesis and dramatically enhances lung metastasis *in vivo*. Role of Cav-1 in cell invasiveness and matrix metalloproteinase (MMP-2/9) secretion. J Biol Chem 2004;279:51630–46.

Tumor Paint: A Chlorotoxin:Cy5.5 Bioconjugate for Intraoperative Visualization of Cancer Foci

Mandana Veiseh, Patrik Gabikian, S-Bahram Bahrami, et al.

Cancer Res 2007;67:6882-6888.